Environ. Sci. Technol. **2007**, *41,* 1218−1224

Hydrologic Flow Controls on Biologic Iron(III) Reduction in Natural Sediments

MORGAN L. MINYARD AND WILLIAM D. BURGOS*

Department of Civil and Environmental Engineering, The Pennsylvania State University, 212 Sackett Building, University Park, Pennsylvania 16802-1408

Bacterial reduction of a hematite-rich natural coastal sand was studied in flow-through column reactors at flow rates which varied from 0.62 to 11 pore volumes d^{-1}. Sand columns were wet-packed with the dissimilatory metal-reducing bacterium (DMRB) *Shewanella putrefaciens* CN32, and a PIPES-buffered, lactate-containing growth medium was pumped through the columns for over 20 days. Soluble Fe(II), acetate and lactate concentrations measured in the column effluents showed that steady-state conditions were established after a few days with every flow rate. The steady-state effluent Fe(II) concentration was directly controlled by the flow rate where $[Fe(II)]_{ss}$ decreased as the flow rate increased. Increased flow rate increased biologic activity based on the steady-state flux of soluble Fe(II) and total Fe(II) production (included Fe-(II) extracted from sand at the conclusion of the experiment), decreased the fraction of lactate oxidized for energy that likely increased cell synthesis, and decreased the concentration of sorbed Fe(II) that, in turn, decreased the relative percentage of Fe(II) retained by the column materials. Increased biologic activity was likely promoted by greater reactant delivery (i.e., lactate, N, P) and greater advective removal of Fe(II). These results demonstrate that biologic Fe(III) reduction, cell growth, and abiotic Fe-(II) sorption are all coupled to the hydrologic flow rate.

Introduction

Iron is the fourth most abundant element in the Earth's crust. Iron(III) in the form of oxides and hydrous oxides and as a structural component of clay minerals is often the most abundant electron acceptor in non-sulfidegenic anaerobic subsurface environments. The iron(II/III) redox couple is also one of the most important redox buffers in anaerobic systems. A variety of dissimilatory metal-reducing bacteria (DMRB) are capable of reductive dissolution of solid-phase Fe(III) minerals coupled to the oxidation of organic acids, alcohols, and hydrogen (*1*−*4*). Biological iron(III) reduction is an important process in natural, contaminated, and engineered systems.

The rate and extent of biological iron(III) reduction is strongly coupled to physical and chemical processes within the environmental system regardless of its complexity. Whether the system is a batch reactor containing a single DMRB pure culture with a single Fe(III) mineral or a field-scale aquifer test containing a diverse microbial community with an assemblage of Fe(III)-bearing minerals, the effects of product accumulation and secondary mineral formation will exert a pronounced effect on Fe(III) reduction. In general, chemical reaction kinetics will slow (or eventually cease) as the free energy of the reaction decreases. The biologic reduction of solid-phase iron(III) (hydr)oxides can also be inhibited by the sorption of biogenic Fe(II) due to the loss of bacterially accessible "free surface sites" (*5*−*7*). Thus, except for Fe(II) sorption to Fe(III) oxides, processes that remove Fe(II) from the system, e.g., by complexation (*8*, *9*), precipitation (*10*), or advective removal (*11*), should promote a greater extent of Fe(III) reduction. A striking example of this was reported by Roden et al. (*11*) where 95% of the Fe-(III) in a goethite-coated sand was bioreduced by the DMRB *Shewanella putrefaciens* CN32 in a flow-through column reactor over 6 months of operation, while only 13% of the Fe(III) was reduced in a 6-month batch incubation conducted in parallel.

While the advective removal of Fe(II) can promote greater reduction of crystalline iron(III) oxides, the added complexity of secondary mineral formation during the reduction of noncrystalline ferrihydrite precludes making a similar generalization. The rate of Fe(II) production, the concentration of Fe(II), the presence and concentration of aqueous species such as HCO_3^-, SO_4^{2-}, and PO_4^{3-} (*12*, *13*), and the hydrologic flow rate (*14*, *15*) can all influence secondary mineral formation. In batch systems, ferrihydrite bioreduction can be enhanced by the precipitation of siderite and/or vivianite or inhibited by Fe(II)-promoted conversion to magnetite (*10*, *12*). In flow-through systems, the flow rate can control the advective flux of Fe(II) that can control the down-gradient profiles of iron minerals that, in turn, can control the final extent of bioreduction (*13*−*15*).

The dissolution of iron(III) (hydr)oxides and associated secondary mineralization pathways are important because these minerals can sorb or sequester substantial amounts of metal contaminants and nutrients. While the stimulation of iron(III) reduction has been proposed for the bioremediation of subsurface environments contaminated with redox active contaminants (e.g., chlorinated solvents, nitroaromatics, metals, and radionuclides), dissolution of contaminant-containing solids may pose the opposite problem. For example, DMRB-mediated reductive dissolution of iron(III) oxides can release sorbed arsenic (*16*−*18*) and sorbed cobalt (*19*). DMRB are also capable of solubilizing metals coprecipitated into either crystalline or noncrystalline ferric oxides (*19*, *20*).

In this study, we have conducted column experiments with a hematite-rich coastal sand wet-packed with a single DMRB pure culture where only the hydrologic flow rate was varied. Our primary objective was to investigate how biologic iron(III) reduction was coupled to the hydrologic flow rate. We demonstrate that biologic activity increased with increased flow rate likely promoted by greater reactant delivery (i.e., lactate, N, P) and greater advective removal of Fe(II). Increased flow rate also decreased Fe(II) sorption that, in turn, could promote iron(III) reduction, and likely increased cell synthesis.

Experimental Section

Iron(III)-Rich Coastal Sand. The natural sediment used was an unconsolidated, sandy-textured, Pleistocene-age Atlantic coastal sediment collected in Eatontown, NJ, and characterized by Zachara et al. (*21*, *22*). This material was selected because the iron(III) mineralogy is dominated by crystalline iron(III) oxides, almost exclusively hematite, that limits

* Corresponding author phone: 814-863-0578; fax: 814-863-7304; e-mail: wdb3@psu.edu.

10.1021/es0619657 CCC: $37.00
Published on Web 01/04/2007

secondary mineral formation, that in turn, simplifies any proposed reaction network used to model this system, and the uniform sand has simple hydrodynamic properties. The red, hematite-rich sand was collected from a depth of 3 meters below ground surface. Based on chemical extractions the majority of iron(III) is crystalline, based on XRD analyses the predominant iron oxide is hematite, and based on electron microscopy hematite exists as grain coatings, microprecipitates, and intergrain cements. The sand was air-dried and passed through a 2-mm sieve prior to characterization and use. The sand has a N_2-BET surface area of 3.1 $m^2\ g^{-1}$ and a dithionite-citrate-bicarbonate (DCB) extractable Fe concentration of 366 umole g^{-1} as reported in (*22*). Moistened sand was autoclaved three times, with 48 h periods between treatments. The sand was then oven dried overnight at 105 °C and stored in a desiccator before use in the experiments.

Synthetic Groundwater. The synthetic groundwater used in these experiments contained 45 mM 1,4-piperazinediethanosulfonic acid (PIPES; pH 6.8), 1 mM $CaCl_2$, 0.1 mM NH_4Cl, 0.01 mM K_2HPO_4, 0.01 mM $MgSO_4$, ca. 9 mM sodium lactate, and 0.1 g L^{-1} yeast extract. Sodium lactate was added as the sole electron donor, and yeast extract was added to provide amino acids and other nutrients required for cell growth. Preliminary experiments demonstrated that yeast extract did not serve as an electron donor or carbon source at this concentration, consistent with earlier reports (*23*). The synthetic groundwater was filtered (0.2-um, cellulose acetate), autoclaved at 121 °C, 15 psi for 15 min and, while still warm, purged overnight with O_2-free N_2. An Alltech OxyTrap (Alltech Associates) was used to remove trace oxygen from the nitrogen gas. As all experiments were conducted under atmospheric O_2-levels on a laboratory bench, the synthetic groundwater feed solution was continuously purged with O_2-free N_2 throughout the experiment to promote and maintain anaerobic conditions in the columns.

Bacterial Inoculum. *Shewanella putrefaciens* strain CN32 (referred to as CN32) was grown aerobically on tryptic soy broth without dextrose at 20 °C on an orbital shaker (100 rpm) (*9*). Cells were harvested by centrifugation (4900 *g*, 10 min, 20 °C) from a 16-hour-old (late-log phase) culture and washed three times in synthetic groundwater that contained no lactate or yeast extract. Cell pellets were resuspended in no-lactate synthetic groundwater and cell density was determined by absorbance at 420 nm. Cell density was adjusted to 10^8 cell mL^{-1} for column inoculation during column packing. No attempt was made to make the bacterial inoculum anaerobic.

Column Packing and Operation. Borosilicate glass chromatography columns (Omnifit; 10-mm dia, 100-mm length) fitted with PTFE end caps (one fixed, one adjustable-length) were used for all experiments. Viton tubing (Masterflex; 1/16-in inner dia, 1/4-in outer dia) was used to connect the columns to a peristaltic pump (Harvard Apparatus) to the synthetic groundwater feed solution and to the effluent sample collection vials.

All columns were "wet packed" such that the water column height above the sand-water interface was constant when incremental masses of sand were added to the column. Synthetic groundwater (containing 10^8 cell mL^{-1} CN32, no lactate or yeast) was always added in an upflow manner to first establish a water column height of 1.0 cm, then 1.0 g of sand was added to the column. The column was tapped on all four sides to remove any air bubbles, and the water column height was re-established to 1.0 cm before another 1.0 g of sand was added. Synthetic groundwater was added slowly such that the sand was never fluidized, and each step proceeded quickly to minimize particle stratification. This procedure was repeated until a total of 9.0 g of sand was added to each column. The adjustable end cap was used to consolidate and secure the sand and yielded an average packed bed length of 7.5-cm. The columns were connected to the peristaltic pump, and ca. 6 pore volumes (PVs) of sterile, anaerobic, lactate-containing synthetic groundwater were pumped through the columns. The experiment then began, presumably under anaerobic conditions, when the desired flow rate was set (defined as $t = 0$ h). Experiments were run at flow rates of 0.619, 2.27, 4.11, and 11.1 PV d^{-1} (1 PV = 2.6 mL). All experiments were conducted with four replicate columns except the no-CN32 controls (4.61 PV d^{-1}) that were conducted with duplicate columns.

Hydrodynamic characteristics of the columns were determined from ^3H tracer breakthrough curves generated in duplicate with two of the columns operated at 11.1 PV d^{-1}. ^3H was spiked into the synthetic groundwater feed solution and measured in effluent fractions by liquid scintillation counting (LKB Wallac). The column PV was defined as the volume displaced between the time when ^3H was statistically greater than the background concentration to the time when ^3H was statistically inseparable from preceding and proceeding values. The column PV was determined to equal 2.60 ± 0.13 mL (equivalent to a porosity of 0.44 vol/vol), and the column dispersivity was 0.01 cm. The replicate ^3H breakthrough curves were essentially indistinguishable suggesting that the column packing procedure produced highly similar columns (Supporting Information Figure S1).

To prevent or minimize Fe(II) oxidation and to preserve organic acids in the column effluent samples, samples were collected daily in plastic scintillation vials containing a measured mass of 1.0 N HCl. Empty plastic vials, vials with HCl, and vials with HCl plus column effluent were all weighed to account for sample dilution and to measure mass flow rate.

Column Destruction. At the end of each experiment, columns were disconnected from the pump and transferred into an anaerobic chamber (Coy, Grass Lakes, MI) for deconstruction. The adjustable end cap was used to force the sand out of the column into plastic scintillation vials. A total of nine samples were collected to characterize the influent, middle, and effluent regions of the column. The three samples from each region were used separately to measure HCl-extractable Fe(II), phosphate-extractable cells, and characterize the iron mineralogy of the sand by room-temperature Mössbauer spectroscopy. HCl-extractable Fe(II) was determined by combining ~1/9 of the column contents (i.e., ~1 g dry sand) with 5 mL of 0.625 N HCl. The HCl-sand suspension was mixed overnight (100 rpm), filtered (0.2 um), and Fe(II) in the filtrate was measured using a modified 1,-10-phenanthroline method. Phosphate-extractable cells were determined by combining ~1/9 of the column contents with 5 mL of 20 mM Na_2HPO_4 (pH 7.0) (*24*). The phosphate-sand suspension was vortex mixed for 1 min, allowed to settle overnight, and cells in the overlying water were enumerated by acridine orange direct counts (AODC). Samples for Mössbauer spectroscopy were dried anaerobically and smeared into a petroleum jelly paste before analysis (*25*, *26*).

Analytical Techniques. Ferrous iron(II) in column effluent and HCl-sand suspension samples was measured using a modified 1,10-phenanthroline method (*27*, *28*). This method specifically includes the addition of ammonium fluoride to complex Fe^{3+} and minimizes its positive interference on color development from Fe^{2+}. The order of reagent addition was important and was conducted as follows: 3.2 mL distilled−deionized water; 0.050 mL concn. HCl; 0.50 mL 0.2-um filtered sample; 0.24 mL 0.73 M ammonium fluoride; 0.50 mL 1,-10-phenanthroline; 0.50 mL 15.5 M ammonium acetate buffer. Fe(II) was measured by absorbance at 510 nm. Lactate and acetate were measured by high performance liquid chromatography (HPLC) with a Waters 2690 HPLC (Milford, MA), equipped with an Ultra Aqueous C18 column (Restek,

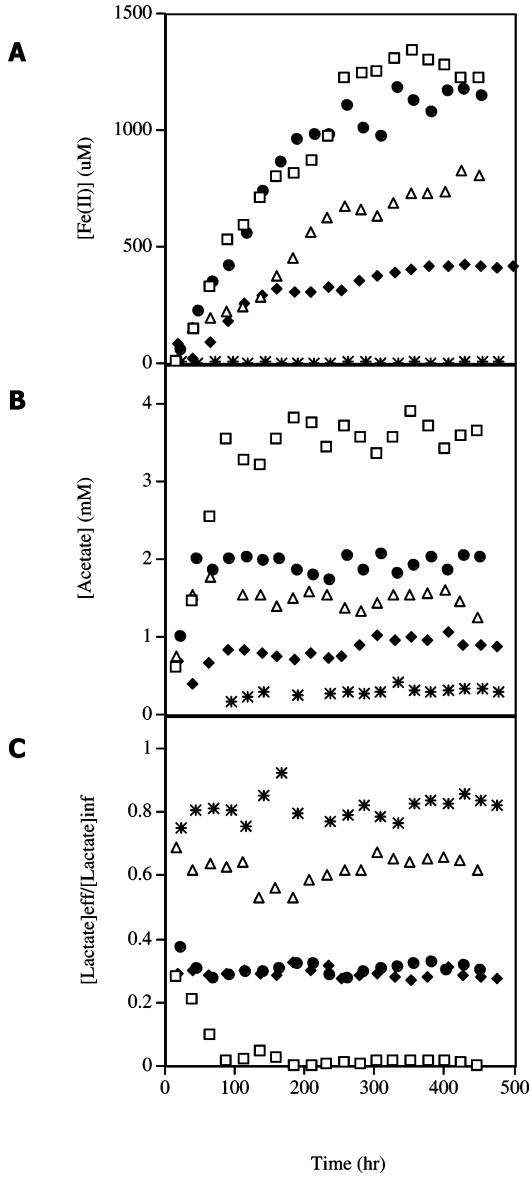

FIGURE 1. Daily effluent concentrations measured from column reactors operated at flow rates of 0.62 pore volumes (PV) d^{-1} (□), 2.3 PV d^{-1} (●), 4.1 PV d^{-1} (△), and 11 PV day^{-1} (◆). Columns were packed with iron(III)-rich sand and *S. putrefaciens* CN32. Uninoculated control columns were operated at a flow rate of 4.4 PV d^{-1} (stars). A) Fe(II), B) acetate, and C) influent-normalized lactate concentrations. Symbols represent mean values from four replicate columns.

Bellefonte, PA), and a Waters 996 photodiode array detector. The mobile phase was a 20 mM phosphate buffer (pH 2.5) and concentrations were determined at 211 nm. The samples (pre-acidified in the effluent collection vials) were filtered (0.2-um), and pH-adjusted to 7.0 with a measured mass of 1.0 N NaOH before HPLC analysis. Cell concentrations were measured by AODC using a Zeiss Axiophot microscope (Jena, Germany) based upon the average from five field counts (each field being 2.64×10^{-4} cm^2) for each slide (three slides per column region).

The statistical analysis program SAS 9.1 (Cary, NC) was used to determine the time at which the effluent Fe(II) and acetate concentrations reached steady-state conditions. The statistical test defined the time at which an effluent analyte concentration converged to a value statistically inseparable from preceding and proceeding values. Convergence criteria were determined at 95% confidence limit by an iterative nonlinear regression fitting of two lines: one for the initial non-steady-state portion and one for the steady-state portion.

Results and Discussion

After several days of operation, the soluble Fe(II), acetate and lactate concentrations in the column effluent approached steady-state conditions (Figure 1). The statistical software package SAS 9.1 (Cary, NC) was used to define the time at which an effluent analyte concentration converged to a value statistically inseparable from preceding and proceeding values. All effluent concentrations measured at and after this time were averaged to calculate the steady-state concentration. The effluent steady-state concentrations for Fe(II), acetate, and lactate produced at the different flow rates tested are summarized in Table 1. Because of slight differences in the influent lactate concentrations for each flow rate, lactate concentrations have been normalized to their respective influent concentrations in Figure 1 (i.e., normalized lactate (mM/mM) = $[Lac]_{eff}/[Lac]_{inf}$). At the flow rate of 0.62 PV d^{-1}, effluent lactate concentrations hovered near the HPLC detection limit (ca. 0.1 mM) such that these columns may have become lactate-limited. Lactate was never limiting at the other flow rates tested. For all flow rates tested, acetate reached its steady-state concentration (65−110 h) before Fe(II) (210 at 280 h). The delayed breakthrough of Fe(II) was likely caused by sorption to the column materials (sand and biomass), whereas acetate and lactate are not expected to sorb to the column materials.

A control column experiment was conducted with autoclaved sediments wet-packed without CN32 but fed sterilized lactate-containing synthetic groundwater. No-CN32 control columns were run at a single flow rate of 4.61 PV d^{-1} and results are in included in Figure 1. Low concentrations of soluble Fe(II), 0.30 uM average, were detected throughout the experiment. At the conclusion of this experiment, sorbed Fe(II) concentrations (eq 5) ranged from 0.29 to 0.44 umol g^{-1}. Soluble acetate, 0.36 mM average, was also detected starting after 96 h of column operation. Substantial concentrations of lactate were consumed within the control reactors during this experiment, where $[\Delta Lac] = \{[Lac]_{inf} - [Lac]_{eff\,ss}\}$ (defined below) averaged 1.63 mM. The production of Fe(II) in the control columns could suggest that the sand contained a natural, small amount of Fe(II). However, the

TABLE 1. Summary of Steady-state Conditions Established in the Column Reactors Operated at Varied Flow Rates[a]

flow rate (mL d^{-1})	flow rate (PV d^{-1})	influent $[Lac]_{inf}$ (mM)	effluent $[Lac]_{eff\,ss}$ (mM)[b]	effluent $[Fe(II)]_{ss}$ (uM) [a]	effluent $[Ace]_{ss}$ (mM)[b]	time to reach $[Ace]_{ss}$ (hr)[c]	time to reach $[Fe(II)]_{ss}$ (hr) [c]
1.61 ± 0.04	0.619	8.85 ± 0.30	0.17 ± 0.10	1270 ± 42	3.58 ± 0.20	110	280
5.89 ± 0.63	2.27	9.06 ± 0.69	2.79 ± 0.15	1090 ± 84	1.95 ± 0.10	65	210
10.7 ± 0.64	4.11	8.63 ± 0.56	5.39 ± 0.37	725 ± 62	1.50 ± 0.12	65	280
28.8 ± 3.1	11.1		5.38 ± 0.30	385 ± 39	0.87 ± 0.11	110	230
12.4 ± 3.8 control	4.61	8.65 ± 0.28	7.03 ± 0.36	0.30 ± 0.40	0.36 ± 0.31		

[a] Values reported as mean ± sd. [b] All effluent concentrations measured at and after steady-state conditions were established were averaged to calculate the steady-state concentration. [c] Steady-state convergence criteria were determined at 95% confidence limit by an iterative nonlinear regression fitting of two lines: one for the initial non-steady-state portion and one for the steady-state portion, using SAS 9.1 (Cary, NC).

corresponding production of acetate and consumption of lactate in the control columns showed that multiple autoclaving did not completely inactivate all native bacterial activity. In batch experiments conducted with identical materials, acetate was not detected in no-CN32 controls over 72 h d incubations (*29*).

Establishment of steady-state conditions appeared to be far more dependent on time of column operation versus number of pore volumes of fluid pumped through the columns (Table 1). For example, the time to reach steady-state effluent Fe(II) concentrations ($t_{ss\ Fe(II)}$) ranged from 210 to 280 h, while the corresponding range of displaced pore volumes ranged from 7.2 to 110 PV. There was no apparent relationship between $t_{ss\ Fe(II)}$ and flow rate. The time to reach steady-state effluent acetate concentrations ($t_{ss\ Ace}$) ranged from 65 to 110 h, while the corresponding range of displaced pore volumes ranged from 2.8 to 51 PV. There was no apparent relationship between $t_{ss\ Ace}$ and flow rate. For all flow rates tested, the ratio of $\{t_{ss\ Ace}/t_{ss\ Fe(II)}\}$ was always >1 and ranged from 2.1 to 4.3 (i.e., acetate always reached steady-state conditions first).

Effect of Flow Rate on Iron(III) Reduction. These experiments were designed to determine how the hydrologic flow rate would affect biologic reactions in the columns, as flow rate was the only experimental variable. The flow rate did not dramatically affect the time required to establish steady-state effluent concentrations of Fe(II) and acetate. For example, while $t_{ss\ Fe(II)}$ varied by a factor of 1.3 and $t_{ss\ Ace}$ varied by a factor of 1.7, the corresponding flow rates varied by a factor of 18. However, the steady-state effluent concentrations, $[Fe(II)]_{ss}$ and $[Ace]_{ss}$, appeared to be directly controlled by the flow rate (Table 1). As the flow rate increased from 0.62 to 11 PV d^{-1}, $[Fe(II)]_{ss}$ decreased from 1270 to 385 uM (factor of 3.3), respectively, and $[Ace]_{ss}$ decreased from 3.58 to 0.87 mM (factor of 4.2), respectively. The steady-state effluent concentrations were used to calculate the steady-state flux of analyte production/consumption:

$$J_{Fe(II)} = Q \times [Fe(II)]_{ss} \quad (1)$$

$$J_{Ace} = Q \times [Ace]_{ss} \quad (2)$$

$$J_{Lac} = Q \times \{[Lac]_{inf} - [Lac]_{eff\ ss}\} \quad (3)$$

where $J_{Fe(II)}$ is the flux of soluble Fe(II) exiting the column (umol d^{-1}), J_{Ace} is the flux of acetate exiting the column (umol d^{-1}), J_{Lac} is the flux of lactate consumed within the column (umol d^{-1}), Q is the average flow rate (L d^{-1}), $[Lac]_{inf}$ is the average lactate concentration entering the column (umol L^{-1}), and $[Lac]_{eff\ ss}$ is the steady-state concentration of lactate exiting the column (umol L^{-1}). The steady-state flux values are plotted as a function of flow rate in Figure 2, and show that biologic activity within the column was strongly coupled to hydrologic conditions.

Assuming that lactate oxidation is used only for cell energy (i.e., no lactate is used for cell synthesis), and that the column materials have reached equilibrium with respect to Fe(II) sorption, the steady-state flux values can be used to compare the measured effluent stoichiometry with the following balanced reaction for incomplete lactate oxidation (CN32 cannot oxidize acetate) coupled to solid-phase hematite (α-Fe_2O_3) reduction:

$$2\ Fe_2O_3 + 1\ CH_3CHOHCOO^- + 7\ H^+ \leftrightarrow$$

$$4\ Fe^{2+} + 1\ CH_3COO^- + HCO_3^- + 4\ H_2O \quad (4)$$

where $CH_3CHOHCOO^-$ and CH_3COO^- are lactate and acetate, respectively. The $J_{Fe(II)}/J_{Ace}$ ratio was in poor agreement with the theoretical 4/1 stoichiometry, and varied from 1/2.8 to 1/1.8 (mol/mol). These calculations, however, are based on the flux of soluble Fe(II) and do not account for solid-associated biogenic Fe(II) retained in the column.

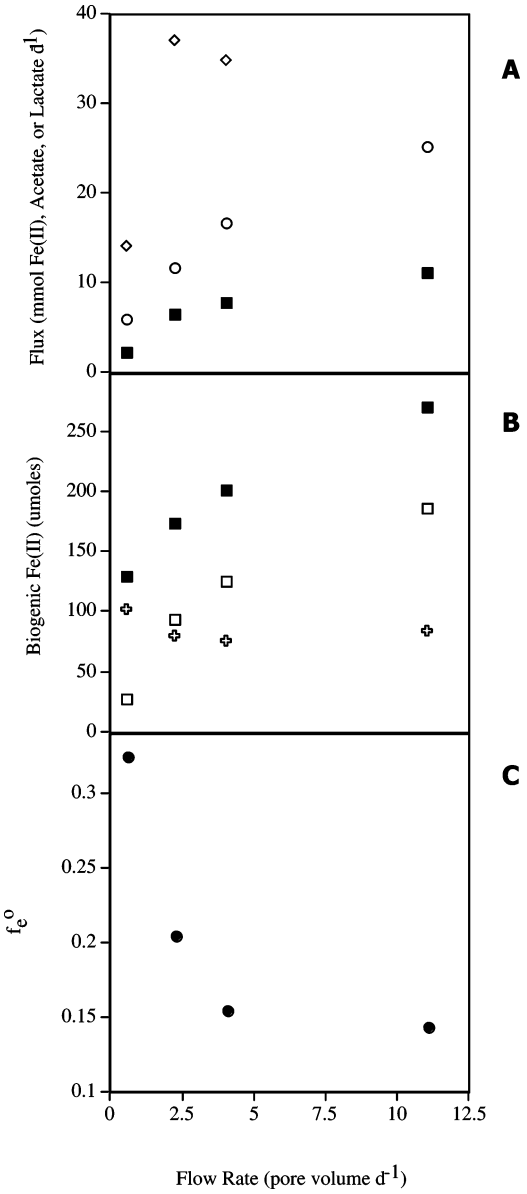

FIGURE 2. (A) Steady-state flux of analyte production/consumption from the column reactors. Flux values of Fe(II) (■), acetate (○) and lactate (◇) were calculated using eqs 1−3, respectively. (B) Distribution of total moles of Fe(II) produced (■) from the column reactors into Fe(II) exported from the columns (□) and Fe(II) retained within the columns (open crosses). C) Fraction of the electron donor oxidized to produce energy (f_e^0) calculated from the stoichiometric ratio of {total Fe(II)}/{total acetate}(mol/mol). Symbols represent mean values from four replicate columns.

Effect of Flow Rate on Iron(II) Sorption. The HCl-extractable Fe(II) concentrations measured at the conclusion of the experiments for the influent, middle and effluent regions of the columns were used to calculate [sorbed Fe(II)]$_{region}$ (umol g^{-1}):

$$[\text{sorbed Fe(II)}]_{region} = \left\{\frac{[\text{HCl Fe(II)}]_{region} - [Fe(II)]_{ss}}{\{M_s/V_w\}}\right\} \quad (5)$$

where $[HCl\ Fe(II)]_{region}$ was the HCl-extractable Fe(II) concentration (umol L^{-1}) measured for one region, $[Fe(II)]_{ss}$ was

TABLE 2. Summary of Biologic Output and Stoichiometric Ratios from the Column Reactors Operated at Varied Flow Rates

flow rate (PV d^{-1})	Fe(II) exported (umol)[a]	Fe(II) retained (umol)[b]	Fe(II) total (umol)[c]	acetate exported (umol)[d]	total Fe(II) / total acetate (umol/umol)[e]	$[\Delta lactate]_{ss}$ / $[Ace]_{ss}$ (mM/mM)[f]
0.619	27.8	102	130	100	1.30	2.43
2.27	93.6	80.2	174	212	0.82	3.22
4.11	126	75.0	201	322	0.62	2.16
11.1	187	83.5	271	471	0.58	
4.61 control	0.07	3.42	3.49	53.9	0.06	4.48

[a] Fe(II) exported = Σ [effluent Fe(II)]$_i$ × (the displaced water volume each day i). [b] Fe(II) retained = [column-averaged sorbed Fe(II)] × (total sand mass). [c] Fe(II) total = moles Fe(II) exported + moles Fe(II) retained. [d] Acetate exported = Σ [effluent Ace]$_i$ × (the displaced water volume each day i). [e] Stoichiometric ratios based on total analyte production of the 20 d experiment. [f] Stoichiometric ratios based on steady-state effluent concentrations established during the 20 d experiment. $[\Delta lactate]_{ss} = \{[Lac]_{inf} - [Lac]_{eff\ ss}\}$.

assumed to be the average Fe(II) concentration in the pore fluids at the time of HCl extraction (umol L^{-1}), M_s was the mass of sand in the column (g), and V_w was the volume of water in the column (L). It should be noted that this operational definition would not distinguish between Fe(II) sorption to sediment minerals or cell surfaces. Equilibrium speciation modeling confirmed that the formation of secondary Fe(II) minerals (e.g., siderite or vivianite) were insignificant in these experiments. The total sorbed amount of Fe(II) retained in the column (umol) at the conclusion of the experiment was

$$M_{Fe(II)\ retained} = [\text{sorbed Fe(II)}]_{avg} \times M_s \quad (6)$$

where $[\text{sorbed Fe(II)}]_{avg}$ was averaged across the column (umol g^{-1}). The total amount of Fe(II) exported throughout column operation (umol) was

$$M_{Fe(II)\ exported} = \Sigma\ [\text{effluent Fe(II)}]_i \times \Delta V_{w,i} \quad (7)$$

where $[\text{effluent Fe(II)}]_i$ was the soluble Fe(II) concentration measured each day *i* (umol L^{-1}), and $\Delta V_{w,i}$ was the volume of water displaced each day *i* (L). Similarly, the total amount of acetate exported throughout column operation (umol) was

$$M_{Ace\ exported} = \Sigma\ [\text{effluent Ace}]_i \times \Delta V_{w,i} \quad (8)$$

where $[\text{effluent Ace}]_i$ was the soluble acetate concentration measured each day *i* (umol L^{-1}).

Total mole quantities of biologic output from the different column experiments are summarized in Table 2. Total biologic output was linearly correlated to the hydrologic flow rate (Figure 2B; $R^2 = 0.95$ with y-intercept $\neq 0$ for $M_{Fe(II)\ total}$ vs flow rate). Increased biologic activity would likely be promoted by greater reactant delivery (i.e., lactate, N, P) and greater advective removal of Fe(II) (*11*). These data reveal that the relative percentage of Fe(II) retained by the column materials (i.e., $M_{Fe(II)\ retained}/M_{Fe(II)\ total}$) was also strongly coupled to hydrologic conditions. Increased flow rate increased biologic activity based on the steady-state flux of soluble Fe(II) and based on $M_{Fe(II)\ total}$ (Figure 2), but decreased [sorbed Fe(II)] (Figure 3) which decreased $M_{Fe(II)\ retained}$.

Increased Fe(II) sorption at the low flow rates was most likely caused by the corresponding increased aqueous Fe(II) concentrations contained in the pore fluids. Within the columns, the lowest [sorbed Fe(II)] values were measured in the effluent region and higher concentrations were measured in the influent and middle regions (Figure 3A). Greater differences in [sorbed Fe(II)] values between the column regions occurred at higher flow rates. A large series of batch bioreduction experiments were conducted using the same sediments, CN32, growth buffer, and employing the same analytical and calculation techniques, and the results were used to generate the Fe(II) sorption isotherm shown in Figure 3B (*29*). The data for the column experiments were obtained from the steady-state effluent Fe(II) concentrations and the final column-averaged sorbed Fe(II) concentrations. The overlay of the column reactor sorption data onto the batch reactor-derived Fe(II) sorption isotherm demonstrate that sorption equilibria was achieved in the columns over 20 d. This implies that the reactions of Fe(II) with sediment materials (i.e., sorption or desorption) in the columns were not mass transport or kinetically limited under any flow rate in these column experiments.

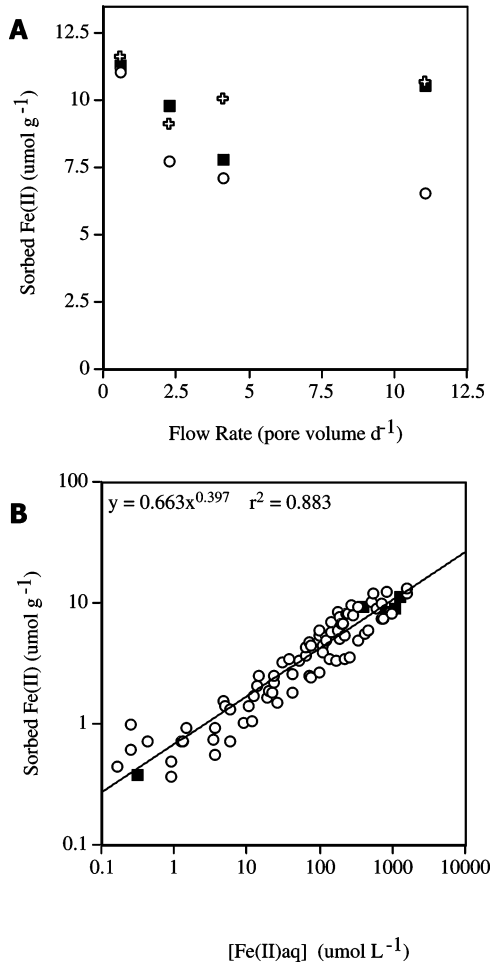

FIGURE 3. (A) Distribution of sorbed Fe(II) between influent (■), middle (open crosses), and effluent regions (○) within the columns. (B) Fe(II) sorption isotherm for iron(III)-rich sand generated from a large series of batch reactor experiments (open symbols). Regression equation used to fit Freundlich isotherm to batch-derived data (solid line). Column reactor sorption data (■) obtained from steady-state effluent Fe(II) concentrations and column-averaged sorbed Fe(II) concentrations.

Effect of Flow Rate on Iron(II)/Acetate Stoichiometric Ratio. The reaction stoichiometry presented in eq 4 can also be compared to the total mole quantities of Fe(II) and acetate produced (Table 2). The $M_{Fe(II)\ total}/M_{Ace\ exported}$ ratio decreased nonlinearly from 1.3/1 to 0.58/1 (mol/mol) as the flow rate increased from 0.62 to 11 PV d^{-1}. However, the utilization of lactate for cell synthesis would directly affect the stoichiometry of eq 4. A generic model for the bioenergetics of incomplete lactate oxidation coupled to solid-phase hematite reduction can be constructed from the following reactions using the framework presented by Rittman and McCarty (*30*):

$$R_d:\ 5CH_3COO^- + 5HCO_3^- + 25H^+ + 20e^- \leftrightarrow 5CH_3CHOHCOO^- + 10H_2O \quad (9)$$

$$R_a:\ 10Fe_2O_3 + 60H^+ + 20e^- \leftrightarrow 20Fe^{2+} + 30H_2O \quad (10)$$

$$R_c:\ 5HCO_3^- + NH_4^+ + 24H^+ + 20e^- \leftrightarrow C_5H_7O_2N + 13H_2O \quad (11)$$

where R_d is the $^1/_2$ cell reduction reaction for the electron donor (all reactions have been normalized to a common quantity of $20e^-$), R_a is the $^1/_2$ cell reduction reaction for the electron acceptor, and R_c is the $^1/_2$ cell reduction reaction for cell biosynthesis. An overall balanced reaction, R, that accounts for the fraction of the electron donor oxidized to produce energy (f_e^0) and for the fraction of the electron donor used for cell biosynthesis (f_s^0), where $f_e^0 + f_s^0 = 1$, can be derived to equal

$$R = f_e^0 \times R_a + f_s^0 \times R_c + R_d \quad (12)$$

The designation of f_e^0 and f_s^0 are used to denote that these processes have not been corrected for endogenous decay (*30*).

The stoichiometric ratios of $M_{Fe(II)\ total}/M_{Ace\ exported}$ measured in these experiments were used to calculate f_e^0 as a function of flow rate and the results are presented in Figure 2C. $M_{Fe(II)\ total}/M_{Ace\ exported}$ ratios of 1.30−0.58 predicted f_e^0 values of 0.33−0.14 for flow rates that varied from 0.62 to 11 PV d^{-1}, all respectively. Batch studies of the growth of *Shewanella algae* with lactate as the electron donor and Fe(III)-citrate as the electron acceptor have been used to estimate an f_e^0 value of ca. 0.65 (personal communication, Eric Roden), and do not agree well with our low f_e^0 values. In addition, the flux ratios of J_{Lac}/J_{Ace} do not agree well with the theoretical 1/1 stoichiometry (constant independent of f_e^0), but varied from 2.2/1 to 3.2/1 (mM/mM) with no apparent trend with flow rate. While we cannot fully explain discrepancies between the stoichiometries of Fe(II)/acetate and lactate/acetate compared to expected results, the trend between the calculated fraction of electron donor used for cell growth (f_e^0) and the hydrologic flow rate is quite interesting. This relationship suggests that cell synthesis would have increased with increased flow rate. Final biomass concentrations based on phosphate-extracted cell counts showed only slight variability as a function of flow rate (Supporting Information Figure S2). Final biomass concentrations ranged from 5×10^7 to 6×10^8 cell mL^{-1} for all experiments and did not increase with flow rate. However, a large portion of biomass could have been exported in the column effluent as reported in ref *11*. Effluent biomass concentrations could not be measured in this study because of the required acid-preservation of the effluent samples.

Environmental Implications. These experiments clearly demonstrated that biologic Fe(III) reduction, abiotic Fe(II) sorption, and likely cell synthesis are all coupled to the hydrologic flow rate in a complex manner. The stimulation of biological Fe(III) reduction has been proposed and used for the remediation of soil and groundwater contaminated with a variety of reducible inorganic (e.g., Cr(VI), Tc(VII), and U(VI)) and organic contaminants (e.g., chlorinated solvents and trinitrotoluene). In situ redox barriers such as Fe(II)-enriched zones can be created by stimulation of DMRB (*31*), chemical reduction (e.g., dithionite (*32*)) or emplacement of reduced solids (e.g., Fe(0) filings (*33*)). The flux of reducible contaminants flowing into the redox barrier should govern the design of the system such that, to the greatest extent possible, the flux of reducing equivalents generated (and regenerated) within the barrier slightly exceed the contaminant flux. For a DMRB-mediated bio-barrier, the flux of soluble biogenic Fe(II) will be dependent on the flux of organic donor addition. Because Fe(II) sorption to Fe(III) (hydr)-oxides can inhibit further Fe(III) reduction and can be dependent on hydrologic flow rate, the flow rate through the barrier will also control the flux of soluble biogenic Fe(II) in a complicated feedback manner. A better understanding of the effect of hydrology on this type of biologic activity will be required to optimize the design of these types of in situ treatment systems.

Acknowledgments

This research was supported by the Natural and Accelerated Bioremediation Research Program (NABIR), Office of Biological and Environmental Research (OBER), Office of Energy Research, U.S. Department of Energy (DOE) through grant no. DE-FG02-04ER63914 to The Pennsylvania State University, and was partially supported by the Penn State Biogeochemical Research Initiative for Education (BRIE) sponsored by NSF (IGERT) grant DGE-9972759. We thank Nicole DeNovio for demonstrations of her wet-packing column technique, Eric Roden for discussions on microbial bioenergetics, and three anonymous reviewers for their helpful comments.

Supporting Information Available

Hydrodynamic analysis of ^3H breakthrough curves from two of the columns operated at 11.1 PV d^{-1}. Final biomass concentrations and distributions measured at the conclusion of the column experiments. This material is available free of charge via the Internet at http://pubs.acs.org.

Literature Cited

(1) Myers, C. R.; Nealson, K. H. Bacterial manganese reduction and growth with manganese oxide as the sole electron acceptor. *Science* **1988,** *240*, 1319−1321.

(2) Lovley, D. R.; Philips, E. J. P. Novel mode of microbial energy metabolism: Organic carbon oxidation coupled to dissimilatory reduction of iron or manganese. *Appl. Environ. Microbiol.* **1989,** *54*, 1472−1480.

(3) Fredrickson, J. K.; McKinley, J. P.; Bjornsatd, B. N.; Ringleberg, D. B.; White, D. C.; Krumholz, L. R.; Suflita, J. M.; Colwell, F. S.; Lehman, R. M.; Phelps, T. J. Pore-size constraints on the activity and survival of subsurface bacteria in a late Cretaceous shale-sandstone sequence, northwester New Mexico. *Geomicrobiol. J.* **1997**, *14*, 183−202.

(4) Caccavo, F. Jr., Lonergan, D. J.; Lovley, D. R.; Davis, M.; Stolz, J. F.; McInerney, M. J. Geobacter sulfurreducens sp. nov., a hydrogen- and acetate-oxidizing dissimilatory metal-reducing microorganism. *Appl. Environ. Microbiol.* **1994**, *60*, 3752−3759.

(5) Roden, E. E.; Urrutia, M. M. Ferrous iron removal promotes microbial reduction of crystalline iron(III) oxide. *Environ. Sci. Technol.* **1999**, *33*, 1847−1853.

(6) Burgos, W. D.; Fang, Y.; Royer, R. A.; Yeh, G.-T.; Stone, J. J.; Jeon, B.-H.; Dempsey, B. A. Reaction-based modeling of quinine-mediated bacterial iron(III) reduction. *Geochim. Cosmochim. Acta.* **2003**, *67*, 2735−2748.

(7) Liu, C.; Kota, S.; Zachara, J. M.; Fredrickson, J. K.; Brinkman, C. K. Kinetic analysis of the bacterial reduction of goethite. *Environ. Sci. Technol.* **2001**, *35*, 2482−2490.

(8) Urrutia, M. M.; Roden, E. E.; Zachara, J. M. Influence of aqueous and solid-phase Fe(II) complexants on microbial reduction of crystalline Fe(III) oxides. *Environ. Sci. Technol.* **1999**, *33*, 4022−4028.
(9) Royer, R. A.; Burgos, W. D.; Fisher, A. S.; Dempsey, B. A.; Unz, R. F. Enhancement of biological reduction of hematite by electron shuttling and Fe(II) complexation. *Environ. Sci. Technol.* **2002**, *36*, 1939−1946.
(10) Fredrickson, J. K.; Zachara, J. M.; Kennedy, D. W.; Dong, H.; Onstott, T. C.; Hinman, N. W.; Li, S.-M. Biogenic iron mineralization accompanying the dissimilatory reduction of hydrous ferric oxide by a groundwater bacterium. *Geochim. Cosmochim. Acta.* **1998**, *62*, 3239−3257.
(11) Roden, E. E.; Urrutia, M. M.; Mann, C. J. Bacterial reductive dissolution of crystalline Fe(III) oxide in continuous-flow column reactors. *Appl. Environ. Microbiol.* **2000**, *66*, 1062−1065.
(12) Zachara, J. M.; Kukkadapu, R. K.; Fredrickson, J. K.; Gorby, Y. A.; Smith, S. C. Biomineralization of poorly crystalline Fe(III) oxides by dissimilatory metal reducing bacteria (DMRB). *Geomicrobiol. J.* **2002**, *19*, 179−207.
(13) Hansel, C. M.; Benner, S. G.; Fendorf, S. Competing Fe(II)-induced mineralization pathways of ferrihydrite. *Environ. Sci. Technol.* **2005**, *39*, 7147−7153.
(14) Benner, S. G.; Hansel, C. M.; Wielenga, B. W.; Barber, T. M.; Fendorf, S. Reductive dissolution and biomineralization of iron hydroxide under dynamic flow conditions. *Environ. Sci. Technol.* **2002**, *36*, 1705−1711.
(15) Hansel, C. M.; Benner, S. G.; Neiss, J.; Dohnalkova, A.; Kukkadapu, R. K.; Fendorf, S. Secondary mineralization pathways induced by dissimilatory iron reduction under advective flow. *Geochim. Cosmochim. Acta.* **2003**, *67*, 2977−2992.
(16) Cummings, D. E.; Caccavo, F. Jr.; Fendorf, S.; Rosenzweig, R. F. Arsenic mobilization by the dissimilatory Fe(III)-reducing bacterium Shewanella alga BrY. *Environ. Sci. Technol.* **1999**, *33*, 723−729.
(17) Zobrist, J.; Dowdle, P. R.; Davis, J. A. Oremland, R. S. Mobilization of arsenite by dissimilatory reduction of adsorbed arsenate. *Environ. Sci. Technol.* **2000**, *34*, 4747−4753.
(18) Smedley, P. L.; Kinniburgh, D. G. A review of the source, behaviour and distribution of arsenic in natural waters. *Appl. Geochem.* **2002**, *17*, 517−568.
(19) Zachara, J. M.; Fredrickson, J. K.; Smith, S. C.; Gassman; P. L. Solubilization of Fe(III) oxide-bound trace metals by a dissimilatory Fe(III) reducing bacterium. *Geochim. Cosmochim. Acta.* **2001**, *65*, 75−93.
(20) Fredrickson, J. K.; Zachara, J. M.; Kukkadapu, R. K.; Gorby, Y. A.; Smith, S. C.; Brown, C. F. Biotransformation of Ni-substituted hydrous ferric oxide by an Fe(III)-reducing bacterium. *Environ. Sci. Technol.* **2001**, *35*, 703−712.
(21) Zachara, J. M.; Smith, S. C.; Kuzel, L. S. Adsorption and dissociation of Co-EDTA complexes in Fe oxide-containing subsurface sands. *Geochim. Cosmochim. Acta.* **1995**, *59*, 4825−4844.
(22) Zachara, J. M.; Fredrickson, J. K.; Li, S.-M.; Kennedy, D. W.; Smith, S. C.; Gassman, P. L. Bacterial reduction of crystalline Fe^{3+} oxides in single phase suspensions and subsurface materials, *Am. Mineral.* **1998**, *83*, 1426−1443.
(23) Roden, E. E.; Lovely, D. R. Dissimilatory Fe(III) Reduction by the marine microorganism *Desulfuromonas acetoxidans. Appl. Environ. Microbiol.* **1993**, *59*, 734−742.
(24) Zuberer, D. A. *Recovery and Enumeration of Viable Bacteria. Methods of Soil Analysis: Part 2 Microbiological and Biochemical Properties*; Mickelson, S. H., Ed.; Madison, WI, Soil Science Society of America, Inc: Madison, WI, 1994; pp 124−129.
(25) Jang, J. H.; Dempsey, B. A.; Catchen, G. L.; Burgos, W. D. Effects of Zn(II), Cu(II), Mn(II), NO_3^-, or SO_4^{2-} at pH 6.5 and 8.5 on transformation of hydrous ferric oxide (HFO) as evidenced by Mössbauer spectroscopy. *Colloids Surf. A* **2003**, *221*, 55−68.
(26) Kukkadapu, R. K.; Zachara, J. M.; Smith, S. C.; Fredrickson, J. K.; Liu, C. Dissimilatory bacterial reduction of Al-substituted goethite in subsurface sediments. *Geochim. Cosmochim. Acta.* **2001**, *65*, 2913−2924.
(27) Tamura, H.; Goto, K.; Yotsuyanagi; T.; Nagayamar, M. Spectrophotometric determination of iron(II) with 1,10-phenanthroline in the presence of large amounts of iron(III). *Talanta* **1973**, *21*, 314−318.
(28) Jeon, B. H.; Dempsey, B. A.; Burgos, W. D.; Royer, R. A. Reactions of ferrous iron with hematite. *Colloids Surf. A* **2001**, *191*, 41−55.
(29) Minyard, M. L. Kinetics of biological iron(III) reduction of natural sediments in batch and column reactors. M. S. Thesis, The Pennsylvania State University, University Park, PA.
(30) Rittmann, B. E.; McCarthy, P. L. *Environmental Biotechnology: Principles and Applications*; McGraw Hill: New York, 2001.
(31) Anderson, R. T.; Vrionis, H. A.; Ortiz-Bernad, I.; Resch, C. T.; Long, P. E.; Dayvault, R. et al. Stimulating in situ activity of Geobacter species to remove uranium from the groundwater of a uranium-contaminated aquifer. *Appl. Environ. Microbiol.* **2003**, *69*, 5884−5891.
(32) Amonette, J. E.; Szecsody, J. E.; Schaef, H. T.; Templeton, J. C.; Gorby, Y. A.; Fruchter, J. S. 1994. Abiotic Reduction of Aquifer Materials by Dithionite: A Promising In Situ Remediation Technology. In *In Situ Remediation: Scientific Bases for Current and Future Technologies*, Proceedings of the 33rd Hanford Symposium on Health and the Environment; Battelle Press: Richland, WA, 1994; pp 851−882.
(33) U.S. Environmental Protection *Agency. Permeable Reactive Subsurface Barriers for the Interception and Remediation of Chlorinated Hydrocarbon and Chromium(VI) Plumes in Ground Water*; EPA/600/F-97/008; U.S. Government Printing Office: Washington, DC, 1997.

Received for review August 15, 2006. Revised manuscript received November 28, 2006. Accepted November 29, 2006.

ES0619657